Modelling bi-static uncertainties in sequential Monte Carlo with the GLMB model

Murat Üney, Alexey Narykov, Jason Ralph, Simon Maskell
School of Electrical Engineering, Electronics and Computer Science
University of Liverpool, L69 3BX, Liverpool, UK
Emails:{M.Uney, A.Narykov, jfralph, smaskell}@liverpool.ac.uk

***Abstract*—Bi-static sensing, where the transmitter and receiver of sensors are separately located, underlies a wide range of collaborative sensing systems. Bi-static detections generally feature a signal time-of-flight (ToF) and an angle-of-arrival (AoA). The current practice in multi-object tracking uses the bi-static geometry to map these pairs onto a selected coordinate frame and filter the mapped detections with a noisy range-bearing (i.e., a mono-static) sensor model. However, the uncertainties in ToF-AoA pairs are not equivalently captured by this model, and the sensing geometry may result in significant degradation of the modelling accuracy. We introduce bi-static likelihood and false alarm models together with Monte Carlo (MC) computational methods to accurately capture the uncertainties involved and use them within Bayesian filtering. We demonstrate the efficacy of our proposed model in simulations with multiple objects using a sequential MC version of the generalised labelled multi-Bernoulli (GLMB) track filter. We compare the filtering performance with the conventional approximation mentioned above.**

I. Introduction

Situational awareness in both defence and non-defence contexts benefits from separately placed transmitter and receiver nodes. These systems provide spatial diversity that improve the sensing performance [1], [2], flexibility in resource use, and, robustness against failures. Example applications include underwater surveillance using multi-static sonar networks [3]–[5] (including 'dipping' sonars and sonobuoys deployed from helicopters), counter rocket-artillery-mortar (CRAM) applications [6], and urban air space control with multi-static radars [7].

Each separately located transmitter/receiver pair in these systems form a bi-static pair as the atomic active sensing unit to consider when processing the signals [8]. In this work, we consider Bayesian filtering of detections from bi-static pairs and estimating the number of objects and their trajectories, i.e., bi-static tracking, motivated by the above mentioned applications.

Coupled with a bi-static detection are estimates of the angle-of-arrival (AoA) and time-of-flight (ToF) of the signal that has led to the detection. The AoA is the angle with which the wavefront of the probing pulse sent by the transmitter has arrived at the receiver after getting reflected by the object of interest, or background reflectors (see, Fig.1). The ToF is the time it took for the probing signal to travel from the transmitter to the reflector and then to the receiver. The product of ToF with the propagation speed is often referred to as the bi-static range.

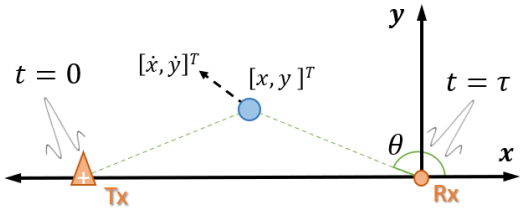

Fig. 1: Bi-static sensing: A transmitter (orange triangle) sends a probing waveform at time zero, a reflector (blue circle) is at $[x, y]^T$ moving with velocity $[\dot{x}, \dot{y}]^T$, and a receiver (orange circle) receives the reflected probe at time τ with wavefront approach angle θ.

Bi-static detections involve uncertainties in these estimates, thus, AoA and ToF are noisy. In addition, some of these detections may be false alarms. Bayesian filtering algorithms take into account these uncertainties through measurement likelihood and clutter models [9], [10]. As a result, the fidelity of these models directly affect the tracking performance.

A common practice in tracking with bi-static detections is to map pairs of AoA and ToF onto the Euclidean plane, i.e., calculate the coordinates of the reflector position in Fig.1, and use range-bearing uncertainty models (see, e.g., [11], [12]). However, conventional likelihood and clutter models in the range-bearing domain are valid for mono-static configurations in which the transmitter and the receiver are co-located. The degradation in modelling accuracy might be small when the reflector is located at a much larger distance compared to the bi-static baseline, i.e., the distance between the transmitter and the receiver. In some applications including underwater sensing, however, such advantageous geometries should not be expected, especially when mobile transmitter and receiver platforms are used [5].

We address modelling of bi-static measurements in Bayesian track filtering by directly relating (ToF, AoA) pairs to the reflector kinematics thereby resolving the discrepancy of the measurement noise model in the above mentioned standard approximation. This also allows us to specify false alarms distribution in the original measurement domain as per the modelling requirements in tracking [13] and avoid false track initiations that stem only from imprecise modelling of false alarms. The result is an endogenous generative model for bi-static detections collected in scans.

The structure of the paper is as follows: In Sec. II we introduce the endogenous bi-static model and compare it

with a standard approximation. We explain how this model is used in multi-object tracking in Sec. III. We demonstrate the efficacy of our approach through a simulation example in Sec. IV, and, finally we conclude.

II. Bi-static Detections and Modelling

In a bi-static system, a transmitter located at x_{tx} probes a region of interest with a waveform (Fig. 1). A receiver located at x_{rx} collects reflected signals from the region and processes the front-end signals to detect reflected replicas by matched filtering [14].

Each detection is associated with the total time for the probing waveform to propagate and reach the reflector and be received at the receiver, i.e., ToF. Let us denote this quantity by τ, the total length of the path by $\tilde{R}$, and the propagation speed by c (assumed constant for simplicty). For a reflector located at x, the ToF is given by

$$\tau = \frac{\big(\|x_{tx} - x\| + \|x_{rx} - x\|\big)}{c}, \tag{1}$$

where $\|.\|$ denotes the l_2 vector norm and the numerator $\tilde{R} \triangleq \tau \times c$ is referred to as the bi-static range. Note that this value is lower bounded by the baseline distance between the transmitter and the receiver R_b. Iso-range curves are hence ellipsoids with x_{tx} and x_{rx} at the foci [15], [16].

In this work we assume that the receiver is capable of finding the AoA of the detected signal wavefronts given by

$$\theta = \measuredangle(x - x_{rx}). \tag{2}$$

Some bi-static systems can measure the Doppler shift of the detected signals and distinguish between returns from moving targets of interest and stationary objects. However, the focus of this paper is on settings where such processing is not available.

Measurement likelihood models relate a state vector $\mathbf{x}$ that is often selected as a concatenation of a location x and a velocity vector $\dot{x}$. The above ToF and AoA equations (1) and (2) specify a bi-static mapping $z = B(x; x_{tx}, x_{rx})$ where $z \triangleq [\tau, \theta]^T$ denotes a bi-static measurement and T is the vector transposition operation. The deviations that lead to errors in τ and θ exhibit the law of large numbers and the errors are normal. Therefore, the likelihood function is given by

$$l(z = (\tau, \theta)|\mathbf{x}; x_{tx}, x_{rx}) = \mathcal{N}(z; B(x; x_{tx}, x_{rx}), \Sigma_B), \tag{3}$$

where the right hand side of the above equation is a bi-variate Gaussian with a covariance of Σ_B. For example, invoking the assumption that the errors in τ and θ are independent leads to a diagonal covariance matrix $\Sigma_B = \text{diag}(\sigma_\tau^2, \sigma_\theta^2)$ where σ_τ^2 and σ_θ^2 are the noise variances in ToF and AoA values, respectively.

The false alarms in Bayesian track filtering algorithms are modelled using a population process on the measurement space which is $\mathcal{Z} = (\tau_{\min}, \tau_{\max}] \times [0, 2\pi)$ where $\tau_{\min} = R_b/c$ is the elapsed time for a transmitted waveform to propagate along the baseline distance from the transmitter directly to the receiver. Often a Poisson distribution with rate λ and uniform spatial distribution over the measurement space $\mathcal{Z}$ are used. Let us denote this distribution by

$$\kappa(z) = Pois(\lambda, \mathcal{U}_{\mathcal{Z}}), \tag{4}$$

where $\mathcal{U}_{\mathcal{Z}}$ denotes a uniform density over $\mathcal{Z}$.

The endogenous bi-static model in (1)–(4) directly fits into the dynamic multi-object models used in Bayesian track filtering [17] as the measurement model.

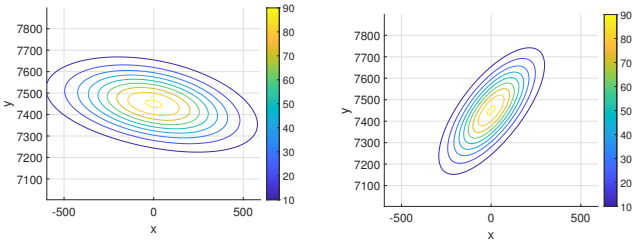

(a) Bi-static likelihood (b) Widely-used surrogate

Fig. 2: Likelihoods evaluated for $(\tau = 10\sqrt{2}c, \theta = 3\pi/4)$ and $\sigma_\tau = 0.1\text{s}, \sigma_\theta = 1\text{rad}$ over a grid of reflector positions in the $x - y$ plane using (a) the endogenous bi-static model (3) for a transmitter and receiver located at $x = -5c$ and $x = 5c$, respectively, and, (b) the surrogate model (5) for a virtually co-located transmitter/receiver located at $x = 5c$.

A. Widely used surrogate likelihood

Most work on bi-static tracking replaces the bi-static measurement pair with the corresponding point on the Euclidean plane. Then a virtual co-located transmitter/receiver pair located at x_{vs} measures the range and bearing of this point. However, the uncertainties in the bi-static domain are not transformed. Instead, the likelihood function used in Bayesian filtering implies that the errors of these virtual measurements are assumed to be normal, i.e.,

$$\begin{aligned} l_S(z|\mathbf{x}) &\triangleq \mathcal{N}\Big(B(y; x_{vs}, x_{vs}); B(x; x_{vs}, x_{vs}), \tilde{\Sigma}_S\Big) \\ y &\triangleq B^{-1}\big(z = [\tau, \theta]; x_{tx}, x_{rx}\big), \end{aligned} \tag{5}$$

with the inverse transform above explicitly given in the Appendix.

It is instructive to compare the bi-static likelihood in (3) and the widely used surrogate in (5). Both likelihoods use a Gaussian template, however, the domain of the distributions are different because the surrogate model transforms the bi-static measurement to a virtual mono-static sensor's measurement parameterised on x_{vs}. When x is much more distant than the bi-static baseline, i.e., $\|x - x_{tx}\| \approx \|x - x_{rx}\| \gg \|x_{rx} - x_{tx}\|$, the region of typical measurements in both likelihoods are similar. However, when this condition is not met, there might be large discrepancies. Moreover, the level of accuracy varies with x_{vs} given x_{rx} and x_{tx} making it impractical to optimise when transmitter/receiver platforms are mobile.

We illustrate a comparative example in Fig. 2. We consider a transmitter located at $x_{tx} = [-5c, 0]^T$ and a receiver at

$x_{rx} = [5c, 0]^T$ with c denoting the propagation speed (see, also Fig. 1). We evaluate the endogenous likelihood in (3) for $z = (10\sqrt{2}c, 3\pi/4)$, $\sigma_\tau = 0.1\text{s}, \sigma_\theta = 1\text{rad}$, and a grid of x over which the likelihood evaluates larger compared to other possible values of x. The resulting contour map is given in Fig. 2a. In order to visually reveal the effects of using the surrogate, we repeat the evaluation with (5) for a virtual co-located transmitter/receiver pair at $x_{vs} = [5c, 0]^T$. The resulting contour map is in Fig. 2b. The uncertainty regions in Fig. 2a and Fig. 2b appear similar to ellipses with almost perpendicular minor and major axes which results in significantly different posterior distributions when these likelihoods are used in a Bayes update.

The surrogate likelihood (5) imposes the use of a different clutter distribution than (4). This distribution is (equivalently) selected to have a uniform spatial distribution over $\mathcal{Z}_S = (0, \tau_{\max}) \times (0, 2\pi]$, instead of $\mathcal{Z}$ defined above which leaves out $[0, \tau_{\min}]$ in its domain. In other words, instead of $\kappa(z)$ in (4),

$$\kappa_S(z) = Pois(\lambda, \mathcal{U}_{\mathcal{Z}_S}) \tag{6}$$

is used in filtering bi-static detection with the surrogate model.

III. Bi-static update in Bayesian tracking

In this section, we address the utilisation of the proposed bi-static model in multi-object filtering and in particular in sequential Monte Carlo (SMC) generalised labelled multi-Bernoulli filtering (GLMB). The measurement likelihood function of the GLMB filter is introduced in Sec. III-A. Important aspects of the filter implementation that recursively computes the filtering posteriors using this likelihood are highlighted in Sec. III-B.

A. Generalised labelled multi-Bernoulli filter [9]

The GLMB model and recursive Bayesian filtering formulae were introduced in [9] to address estimation of target trajectories in a random finite set (RFS) framework. The computational details of the prediction and measurement update equations of the GLMB filter can be found in [18]. For the sake of simplicity, we shall limit the discussion to the multi-object measurement likelihood function which encapsulates all elements directly affected by the sensor modelling and evaluated in the update step.

A population of objects is described by a multi-object state X in an appropriate state space $\mathcal{X}$. At time k, each object with state $(\mathbf{x}, \ell) \in X$, comprising a kinematic state $\mathbf{x}$ and a discrete label ℓ described by its state space $\mathcal{L}$, is detected with probability $p_D(\mathbf{x}, \ell)$, and if so, it produces a measurement whose state is distributed according to a likelihood $l(\cdot|\mathbf{x}, \ell)$. The multi-object observation $Z = \{z_1, \ldots, z_{|Z|}\} \in \mathcal{Z}$ is then the union of measurements of detected objects and Poisson distributed false alarms arriving with intensity κ.

Let $h^X \triangleq \prod_{\mathbf{x}\in X} h(\mathbf{x})$ denote multi-object exponential of the real-valued function h. Under assumptions that the measurements originating from object detections are generated independently from each other, and the false alarms are independent of the detections, the multi-object likelihood is given by [18]

$$g(Z|X) = e^{-\left(\int \kappa(z')\mathrm{d}z'\right)} \kappa^Z \sum_{\theta\in\Theta(L(X))} \left[\psi_Z(\cdot;\theta)\right]^X, \tag{7}$$

$$\psi_Z(\mathbf{x}, \ell; \theta) = \begin{cases} \frac{p_D(\mathbf{x},\ell) l\left(z_{\theta(\ell)}|\mathbf{x},\ell\right)}{\kappa\left(z_{\theta(\ell)}\right)}, & \text{if } \theta(\ell) > 0 \\ 1 - p_D(\mathbf{x}, \ell), & \text{if } \theta(\ell) = 0 \end{cases}. \tag{8}$$

Here, $\theta : \mathcal{L} \to \{0, 1, \ldots, |Z|\}$ is an association map that hypothesises track l generated measurement $\theta(l)$ and imposes the constraint that a single track can generate at most one measurement. p_D is the probability of detection as a function of the target state. It can be selected as zero if $\mathbf{x}$ is on the path between the transmitter and the receiver to account for the receiver being blinded by the direct path signal.

In (7), $\Theta(L(X))$ is the subset of association maps from those labels only in X, i.e., $L(X)$ where $L(\{(\mathbf{x}, \ell)\}) \triangleq \ell$. Thus, GLMB filtering marginalises out all such hypotheses unlike tracking algorithms that find the most likely global association hypothesis [9], in principle. The implementation approach we adopt from [18] uses Murty's algorithm [19] to approximate (weighted) summations of these terms when computing the filtering posterior with the above likelihood.

In summary, the multi-object measurement likelihood in (7), (8) captures a sensor-specific single-object measurement likelihood, detection and false alarm models. In Section IV, we compare the proposed endogenous model $l(z|\mathbf{x}), \kappa(z)$ with the widely used surrogate model $l_S(z|\mathbf{x}), \kappa_S(z)$ in the tracking performance they result when used in (7), (8) .

B. Implementation details

In this paper we are using the SMC (or particle) implementation of the GLMB filter, with details available in [18], [20]. Thus, the filtering update boils down to evaluating the proposed likelihood at the particle points and the false alarm function for the bi-static measurements.

The standard GLMB formulation [18] assumes a priori information on object birth, which is rarely available in practice. Therefore, this paper adopts an adaptive birth model that initiates the birth components from measurement data [21] (for a similar approach, see also [22]).

IV. Example

In this section, we provide an example in which there are four objects moving with almost constant speed, and, a mobile transmitter platform and a receiver both following a clock-wise arc as depicted in Fig. 3. The propagation speed is selected as $c = 1490$ m/s which is one of the typical configurations when using underwater sonar. The transmitter is omni-directional and sends the probing waveform to the environment every 20 seconds. The receiver detects reflections with probability $P_D(x) = 0.95$ (independent of the state, for simplicity) and finds ToF and AoA with standard deviations of $\sigma_\tau = 0.1\text{s}$ and $\sigma_\theta = 1\text{rad}$, respectively. The expected number of false alarms is selected as $\lambda = 5$. We consider 50 scans. The resulting bi-static ToF and AoA measurements are given in Fig. 4a. The

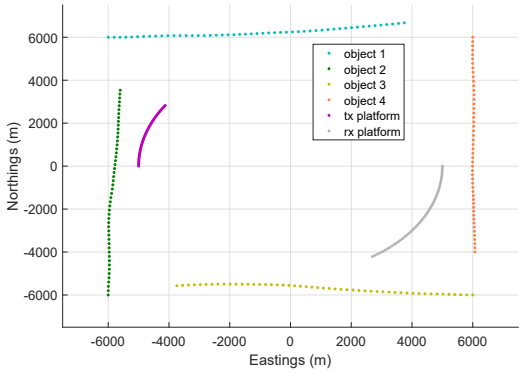

Fig. 3: Multi-object bi-static tracking scenario: Trajectories of the objects, transmitter platform and the receiver platform.

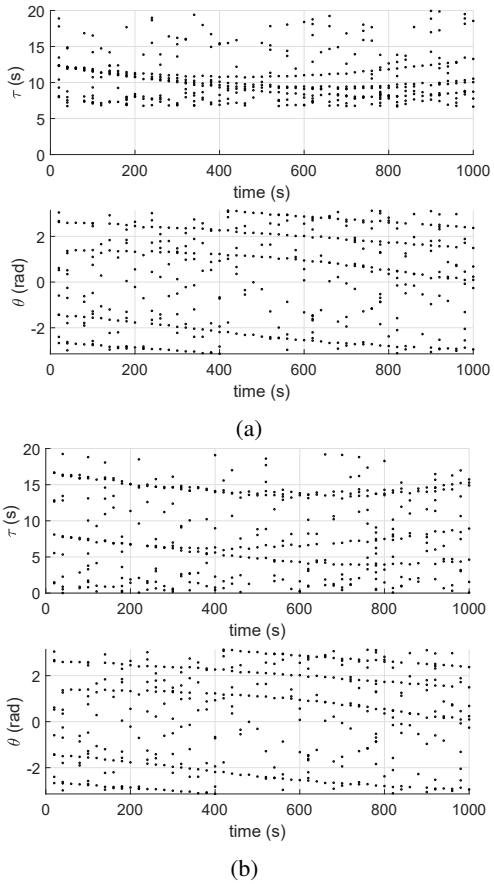

(a)

(b)

Fig. 4: (a) Bi-static ToF and AoA measurements over time. (b) Virtual mono-static ToF and AoA measurements.

ToF is lower bounded by the time it takes for one transmitted pulse to travel directly from the transmitter to the receiver.

First, we use the proposed endogenous likelihood and false alarm model (1)–(4) in GLMB filtering implemented using SMC as detailed in Section III-B. The trajectories output for the bi-static ToF and AoA measurements in Fig. 4a are given in Fig. 5. The results exhibit a reasonable level of accuracy in estimating the number of trajectories and localisation. It is noted that the track continuity for the horizontal northern trajectory is not as good as that for the other three trajectories.

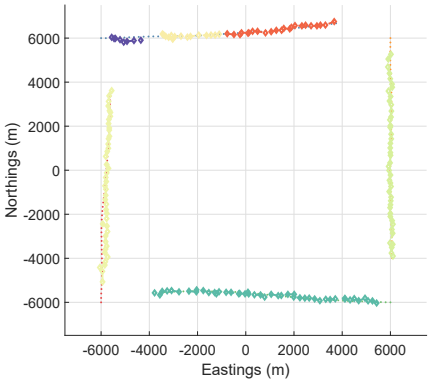

Fig. 5: Estimated trajectories using the endogenous bi-static model in GLMB filtering. Different track labels are depicted with different colours.

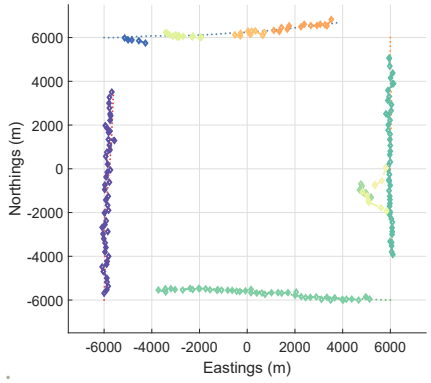

Fig. 6: Estimated trajectories using the surrogate observation model in GLMB filtering. Different track labels are depicted with different colours.

This might be related to the bi-static geometry of this track. Before continuing with the a quantitative assessment of the tracking performance, we present the results obtained using the surrogate model.

The widely-used surrogate model in bi-static processing uses mono-static ToF and AoA measurements as explained in Sec. II. These measurements for a virtual transmitter/receiver pair following the original bi-static receiver's location are given in Fig. 4b. We filter these measurements using the surrogate model in the GLMB filter. The resulting trajectory estimates are given in Fig. 6. Note that there are false trajectories around the vertical track in the East. The track continuity and localisation accuracy for the horizontal track in the North is also worse compared to that obtained by using the proposed approach.

We make a quantitative comparison of the tracking performances by using the OSPA-on-OSPA, or, OSPA2, distance metric for trajectories [23]. OSPA2 satisfies the metric axioms between arbitrary sets of trajectories and penalises track switches along with location and cardinality errors.

First, we evaluate the OSPA2 between the ground truth in Fig. 3 and the estimates output by the proposed model in Fig. 5, and, depict the results in Fig. 7. Specifically, we perform the evaluation for 5 scan long time windows after

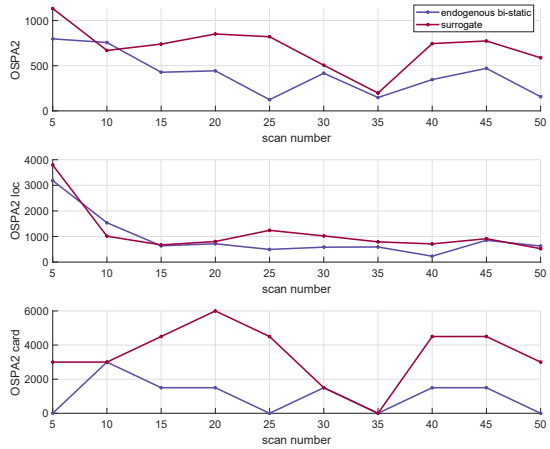

Fig. 7: OSPA2 error metric from the ground truth to the estimated trajectories using the proposed model (blue lines) and the widely-used surrogate (red lines): Total OSPA2 (top), localisation error (mid-pane) and cardinality error (bottom).

partitioning the trajectory sets over time to understand the dynamic behaviour of the errors. The OSPA order and the cut-off parameter used are $p = 1$ and $c = 1500m$, respectively, with the l_2 distance as the base distance. OSPA2 can be decomposed into a localisation error and a cardinality error (i.e., error in the number of trajectories). The total error, localisation error and the are depicted by blue lines in Fig. 7.

Second, we find the error figures for the surrogate model which are given in red lines. The proposed approach consistently performs better than the widely-used surrogate model in terms of localisation accuracy, avoidance to initiating false trajectories and total OSPA2.

V. Conclusions

In this work, we have considered Bayesian filtering of bi-static detections for multi-object tracking and proposed an endogenous likelihood and false alarm model. The modelling assertion is that the errors in the time-of-flight and angle-of-arrival values associated with bi-static detections are Gaussian, but distinct from the usual approximations used for mono-static detections. The model is amenable for Monte Carlo computational methods in Bayesian tracking. In a simulated example, we have demonstrated that the proposed model outperforms a widely-used standard approximation.

Appendix

A. Inverse bi-static mapping B^{-1}

Let us consider the inverse bi-static mapping given by $B^{-1} : (\tau_{min}, \tau_{max}] \times [0, 2\pi) \times \mathbb{R}^2 \times \mathbb{R}^2 \to \mathbb{R}^2$ which maps bi-static measurements to points in the Cartesian space given the location of the transmitter and receiver, i.e., $y = B^{-1}(\tau, \theta; x_{tx}, x_{rx})$. Let us denote the bi-static range of the ToF by $R = c \times \tau$, the unit vector pointing at the AoA by $\mathbf{e} \triangleq [\cos(\theta), \sin(\theta)]^T$, and the bi-static baseline by $\mathbf{b} = x_{tx} - x_{rx}$. Then, the point y on the Euclidean plane that induces the bi-static pair (τ, θ) is found as

$$y = x_{rx} + \frac{R^2 - \mathbf{b}^T\mathbf{b}}{2R - 2\mathbf{b}^T\mathbf{e}}\mathbf{e}. \tag{9}$$

Acknowledgement

The authors would like to thank the UK Defence Science and Technology Laboratories (Dstl, Grant no. 1000143726) for financial support as part of Project BLUE, which is part of the UK MoD University Defence Research Collaboration (UDRC) in Signal Processing.

References

[1] A. M. Haimovich, R. S. Blum, and L. J. Cimini, "MIMO Radar with Widely Separated Antennas," *IEEE Sig. Proc. Mag.*, vol. 25, no. 1, pp. 116–129, 2008.

[2] Y. Pailhas, Y. Petillot, K. Brown, and B. Mulgrew, "Spatially distributed mimo sonar systems: Principles and capabilities," *IEEE Journal of Oceanic Engineering*, vol. 42, no. 3, pp. 738–751, 2017.

[3] R. Tharmarasa, T. Kirubarajan, and T. Lang, "Joint path planning and sensor subset selection for multistatic sensor networks," in *2009 IEEE Symp. on Comp. Int. for Security and Defense App.*, 2009, pp. 51–8.

[4] G. Yang, Y. Li, X. Xiang, and Z. Wang, "Review of development of multi-static sonar for underwater object detection," in *2012 International Conference on Computer Application and System Modeling*, 2012.

[5] G. De Magistris, M. Uney, P. Stinco, G. Ferri, A. Tesei, K. Le Page, "Selective information transmission using convolutional neural networks for cooperative underwater surveillance," the *Proc. of FUSION'20*, 2020, pp. 1–8.

[6] J. F. Ralph and J. M. Davies, "Semi-active guidance using event driven tracking," in the *Proc. of FUSION'11*, 2011, pp. 1–7.

[7] B. Griffin, A. Balleri, C. Baker, and M. Jahangir, "Optimal receiver placement in staring cooperative radar networks for detection of drones," in *2020 IEEE Radar Conference (RadarConf20)*, 2020, pp. 1–6.

[8] J. Li and P. Stoica, Eds., *MIMO Radar Signal Processing*. John Wiley & Sons, 2009.

[9] B. -T. Vo and B. -N. Vo, "Labeled random finite sets and multi-object conjugate priors," *IEEE Trans. on Sig. Proc.*, vol. 61, no. 13, pp. 3460–3475, 2013.

[10] M. Üney, "Type II approximate Bayes perspective to multiple hypothesis tracking," in *the Proc. of FUSION'19*, 2019, pp. 1–8.

[11] F. Meyer, P. Braca, P. Willett, and F. Hlawatsch, "A scalable algorithm for tracking an unknown number of targets using multiple sensors," *IEEE Trans. on Sig. Proc.*, vol. 65, no. 13, pp. 3478–3493, 2017.

[12] D. Gaglione, G. Soldi, F. Meyer, F. Hlawatsch, P. Braca, A. Farina, and M. Z. Win, "Bayesian information fusion and multitarget tracking for maritime situational awareness," *IET Radar, Sonar & Navigation*, vol. 14, pp. 1845–1857(12), December 2020.

[13] B.-N. Vo, M. Mallick, Y. Bar-shalom, S. Coraluppi, R. Osborne, R. Mahler, B. Vo, and J. G. Webster, *Wiley Encyclopedia of Elec. and Electronics Eng.*. J Wiley & Sons, Inc., 2015, ch. Multitarget Tracking.

[14] H. L. V. Trees, *Detection, Estimation, and Modulation Theory: Radar-Sonar Sig. Proc.*. Krieger Pub. Co., Inc., 1992.

[15] N. J. Willis, *Bistatic Radar*, 2nd ed. Scitech Publishing, 2005.

[16] H. Cox, *Underwater acoustic data processing*. Kluwer Academic Publishers, 1989, ch. Fundamentals of bistatic active sonar, pp. 3–24.

[17] E. Delande, M. Üney, J. Houssineau, and D. E. Clark, "Regional variance for multi-object filtering," *IEEE Transactions on Signal Processing*, vol. 62, no. 13, pp. 3415–3428, 2014.

[18] B. Vo, B. Vo, and D. Phung, "Labeled random finite sets and the bayes multi-target tracking filter," *IEEE Transactions on Signal Processing*, vol. 62, no. 24, pp. 6554–6567, 2014.

[19] K. G. Murty, "An algorithm for ranking all the assignments in order of increasing cost," *Oper. Res.*, vol. 16, no. 3, pp. 682–687, 1968.

[20] B. Ristic, M. Beard, and C. Fantacci, "An overview of particle methods for random finite set models," *Inf. Fusion*, vol. 31, pp. 110–126, 2016.

[21] B. Ristic, D. Clark, B.-N. Vo, and B.-T. Vo, "Adaptive target birth intensity for PHD and CPHD filters," *IEEE Transactions on Aerospace and Electronic Systems*, vol. 48, no. 2, pp. 1656–1668, 2012.

[22] S. Lin, B. T. Vo, and S. E. Nordholm, "Measurement driven birth model for the generalized labeled multi-Bernoulli filter," in *2016 Int. Conf. on Cont., Automation and Inf. Sciences (ICCAIS)*. IEEE, 2016, pp. 94–99.

[23] M. Beard, B. T. Vo, and B. Vo, "A solution for large-scale multi-object tracking," *IEEE Trans. on Sig. Proc.*, vol. 68, pp. 2754–2769, 2020.